Preprints.org

Article

Not peer-reviewed version

# The Study Analyzes the Impacts of Pressure the Permeability of Permalloy (Ni81Fe19)1-x(Al2O3)x Thin Films

Mobarek Dib *, Mohammed Elharfaoui *, Mossab Oublal *, Essediq Youssef El Yakoubi *

Posted Date: 23 December 2024

doi: 10.20944/preprints202412.1900.v1

Keywords: Frequency of Resonance; Permalloy Nanoparticles; Permeability; Damping Coefficient

Preprints.org is a free multidisciplinary platform providing preprint service that is dedicated to making early versions of research outputs permanently available and citable. Preprints posted at Preprints.org appear in Web of Science, Crossref, Google Scholar, Scilit, Europe PMC.

Copyright: This open access article is published under a Creative Commons CC BY 4.0 license, which permit the free download, distribution, and reuse, provided that the author and preprint are cited in any reuse.

Preprints.org (www.preprints.org) | NOT PEER-REVIEWED | Posted: 23 December 2024 doi:10.20944/preprints202412.1900.v1

Disclaimer/Publisher's Note: The statements, opinions, and data contained in all publications are solely those of the individual author(s) and contributor(s) and not of MDPI and/or the editor(s). MDPI and/or the editor(s) disclaim responsibility for any injury to people or property resulting from any ideas, methods, instructions, or products referred to in the content.

*Article*

# The Study Analyzes the Impacts of Pressure the Permeability of Permalloy $(Ni_{81}Fe_{19})_{1-x}(Al_2O_3)_x$ Thin Films

**Mobarek Dib [1,*], Mohammed ElHarfaoui [2], Mossab Oublal [1] and Essediq Youssef El Yakoubi [1]**

[1] Laboratory of Condensed Matter Physics and Nanomaterials for Renewable Energy, Faculty of Sciences, University Ibn Zohr, 80000 Agadir, Morocco
[2] Thin Film Laboratory, Physics Department, LPMC, Kenitra-15000, Morocco
* Correspondence: mobarekdib@gmail.com

**Abstract:** Our thin films are constituted by Permalloy nanoparticles the type: $(Ni_{81}Fe_{19})_{1-x}(Al_2O_3)_x$ and Employing Radiofrequency Sputtering, they are deposited on Corning glass substrates in a dynamic field along the hard axis of magnetization, the samples were subjected to a magnetic field applied in their plane. We utilized the ranges of argon pressures of $4.10^{-3}$ and $60.10^{-3}$ (mbar). The rates of $Al_2O_3$ substitution are set at 24, 34 and 44% at. The measurements and damping coefficient deduced from this adjustment align with the calculations of permeability spectra obtained from the Gilbert Lifshitz Landau model. After this adjustment, the damping ratio values accord with the values from the previous research. Similar to pressure, the damping coefficient increases linearly with pressure. A linear relationship exists between the coefficient of depth and the Full Width at Half-Maximum (FWHM) values of the imaginary part of the permeability dependent frequency. The actual fits were done through the convolution of a Gaussian line width for the inhomogeneity term and a Lorentzian line width for the TMS and a magnon-electron (m-e) terms. Based on broadband ferromagnetic resonance measurements of the Permalloy films, the saturation magnetization field ($4\pi Ms$) increase as $H_a$ grew and remained close to the theoretical value. This work helps us understand to the physical origin of the Gilbert damping in magnetic films and utilized in spintronic devices and the sensors applications.

**Keywords:** frequency of resonance; permalloy nanoparticles; permeability; damping coefficient

## 1. Introduction

The Permalloy nanoparticles constitute a rich niche for the study of magnetic recording and related properties. Currently, systems based on alloy matrix with nanoparticles of iron, cobalt or nickel, deposited on metallic substrates, semiconductors, or insulators such as $(Ni_{81}Fe_{19})_{1-x}(Al_2O_3)_x$ are widely investigated. Advancements in 5G communication, high-frequency electronics, and miniaturized devices are driving the accessible for thin films with high saturation magnetization and high permeability. Researchers and engineers are continually exploring and developing new materials and fabrication techniques to meet these demands [1–3]. To put it briefly, The metal-insulator granular films you're discussing consist of magnetic metals (Ni, Co,Fe, and their alloys), non-magnetic elements ,and insulating element. M (non-magnetic elements) and X (insulating elements) are combined to create the insulating matrix [4–8].These soft materials have a dynamic permeability well described by a cyclotron model [9].In particular, the saturation magnetization and anisotropy field are most influential parameters influencing the magnetic behavior of a material, and they play a role in determining its resonance frequency in various applications [10,11]. The assemblies of nanoparticles make it possible to acquire microwave properties which are directly proportional to those of thin film and concentration [12] . The deposits were made by magnetron sputtering under low pressure argon, which provide low anisotropy fields. The growth substrates are Corning glass,

© 2024 by the author(s). Distributed under a Creative Commons CC BY license.

Preprints.org (www.preprints.org) | NOT PEER-REVIEWED | Posted: 23 December 2024 doi:10.20944/preprints202412.1900.v1



permitting detachment of ferromagnetic RF sputtering in a magnetic field employed in the plane of samples. The study of magnetic properties of ferromagnetic deposits was performed before and after peeling on samples that marked the two main axes corresponding to the parallel and perpendicular directions of layer placement during deposition. Applying the permeability spectrum model, gyromagnetism, of Gilbert type parameter is used to determine damping $\alpha_{eff}$. Hysteresis loops captured by vibrating the sample magnetometer (VSM) are employed for identifying the saturation magnetization and anisotropy field. Measuring the permeability as a function of frequency is performed by a disruption technique of microwave coil [13,14].The same measurement method can be applied to a ferromagnetic tape on which a known tensile force is exerted [15].This phenomenon was observed by Grove spraying in 1852 [16].The magnetic field is created by two Helmholtz coils and is applied along to the hard axis magnetization. This measurement procedure was developed in our laboratory[17].

## 2. The Dynamic Equation Landau-Lifshitz- Gilbert (LLG)

The Landau-Lifshitz equation is essential for explaining the dynamics of magnetization in ferromagnetic materials, however for precise modeling of macro-spin dynamics, it is sometimes combined with the Landau-Lifshitz-Gilbert equation [9] which was later reformulated by Gilbert [18] as:

$$\frac{d\vec{M}}{dt} = -\mu_0\gamma\left(\vec{M}\times\vec{H}_{eff}\right) + \frac{\alpha_{eff}}{M_S}\left(\vec{M}\times\frac{d\vec{M}}{dt}\right)$$

The effective field, magnetization, and damping coefficient are symbolized by the letters $\vec{H}$, $\vec{M}$, $\alpha_{eff}$,Consecutively. The Landé g-factor formula is the basis for calculating the gyromagnetic ratio, which is pivotal in describing the behavior of charged particles with spin in a magnetic field [19] **:** $\boldsymbol{\gamma = \frac{g.e}{2m}}$. It appears that your discussion is focused on the properties of films with in-plane uniaxial anisotropy and the use of the macro-spin approximation to solve a specific equation (Eq. 1), The following is how the formulas for $\mu'$ and $\mu''$ are determined [20–22]:

$$\mu' = 1 + 4\pi M_s\gamma^2\frac{\left(H_k^{dyn}+4\pi M_s\right)(\omega_r^2-\omega^2)+\alpha_{eff}^2\omega^2H_k^{dyn}}{(\omega_r^2-(1+\alpha_{eff}^2)\omega^2)^2+\left(\omega\gamma\alpha_{eff}(2H_k^{dyn}+4\pi M_s)\right)^2} \quad (2)$$

$$\mu'' = 4\pi M_s\omega\gamma\alpha_{eff}\frac{\left(H_k^{dyn}+4\pi M_s\right)^2\gamma^2+\left(1+\alpha_{eff}^2\right)\omega^2}{(\omega_r^2-(1+\alpha_{eff}^2)\omega^2)^2+\left(\omega\gamma\alpha_{eff}(2H_k^{dyn}+4\pi M_s)\right)^2} \quad (3)$$

where $\omega_r = 2\pi f_{FMR}$, The saturation magnetization and dynamic magnetic anisotropy field are denoted by the letters $4\pi M_s$ and $H_k^{dyn}$ consecutively. Employing Equations (2) and (3) to adjust the LLG, using permeability spectra to adjust parameters to reduce the difference between theory and experiment.

## 3. Materials and Methods

The composites samples $(Py)_{1-x}$ $(Al_2O_3)_x$ were elaborated from different targets with different surface concentration in $(Py)$ (24%, 34% and 44%). These samples were grown on Corning Glass substrate using a radiofrequency sputtering apparatus (f = 13.56 MHz), of the type LEYBOLD AG Z400. These films were deposited on 9 mm square glass substrates. During deposition, the substrates were placed on the anode, between two magnets creating a magnetic field of 300 Oe to elicit a direction of easy magnetization in the material. For each target, the samples were deposited using a wide range of argon pressures, ranging from $1.9.10^{-3}$ (mbar) to $6.10^{-2}$ (mbar). The film thicknesses for all samples were around 300 nm. Magnetization loops can provide insights into various magnetic properties, including saturation magnetization and coercive field. According to the statement, the

Preprints.org (www.preprints.org) | NOT PEER-REVIEWED | Posted: 23 December 2024 doi:10.20944/preprints202412.1900.v1



sample permeability spectra were obtained at a wide frequency range (250 MHz to 10 GHz) by utilizing a method that involved shorted micro-strip transmission line perturbation [23].

## 4. Results

Vibration sample magnetometer (VSM) is a common and effective approach in materials science and physics, where static magnetic properties of samples can be characterized through magnetic hysteresis loop measurements at room temperature [24–28]. A Figure 1 describes magnetic hysteresis loops ($\boldsymbol{M-H}$ loops) of certain samples. The information you provided indicates that the loops were measured within a magnetic field range between -10 and 10 ($\boldsymbol{kOe}$).The magnetic properties being studied can be influenced by pressure as the observed uniaxial magnetic anisotropy in Figures 1.a and 1.b becomes more prominent at P = $10.10^{-3}$ (mbar).Plotting static parameters from hysteresis loops is depicted in Fig (3-a),Some static parameters from the hysteresis loops are plotted in Fig.3.a, They take care of coercivity for the easy axis ($\boldsymbol{H_{ce}}$) and the hard axis ($\boldsymbol{H_{ch}}$), Static anisotropy field ($\boldsymbol{H_a}$) is the anisotropy field derived from static measurements. Along the hard and easy axes, the difference in magnetic fields crucial for saturation magnetization is characterized as the anisotropy field $\boldsymbol{H_k^{Stat}}$,and it is presented to quantitatively explain the change of magnetic anisotropy, respectively $\boldsymbol{H_k^{Stat} = H_{Sat}^{HA} + H_{Sat}^{EA}}$ [29–31]and is deduced from the HA the rotational-like magnetization curve's incline[32,33]. The hysteresis loops along the $(Py)_{1-x}(Al_2O_3)_x$ thin film's easy and hard axes are visible in Figs. 1.a and 1.b. In deposition, the easy axis direction is the direction of the magnetic field, whereas the hard axis is within the sample plane but perpendicular to the easy axis[34]. Magnetic anisotropy is illustrated by a slanted loop in the hard axis and an exchange bias by a loop shift in the easy axis on the magnetization curve [21,34,35] . The hysteresis loop permits the extraction of the static magnetic anisotropy $\boldsymbol{H_k^{stat}}$ [21,35].

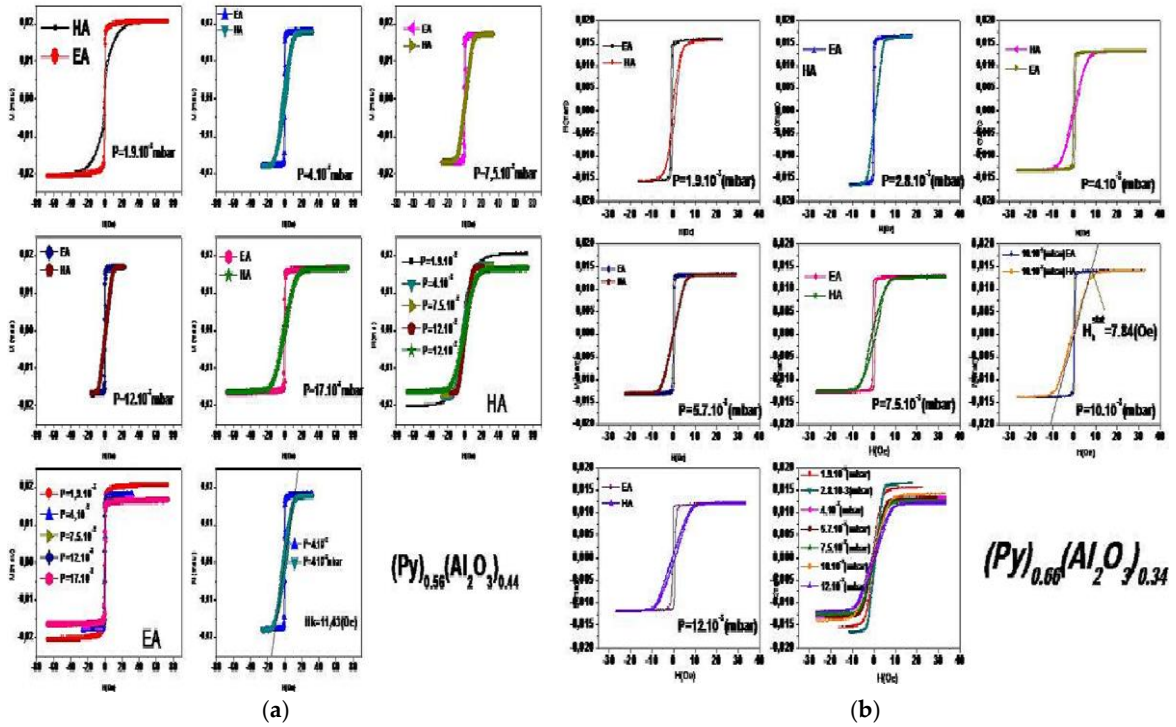


**Figure 1.** represents $M/Ms - H$ loop parts measured within -10 to 10 Oe field range, parallel to easy and hard axis at Permalloy $(Py)_{1-x}(Al_2O_3)_x$ , under different pressures.

In the microwave frequencies range 250 MHz - 1 GHz, the permeability spectra didn't present the resonance at all argon pressures with concentration of 24%. Figure 2.a,2.b shows a similar comparison between experimental and theoretical spectra, illustrating that an increase in pressure leads to a reduction in measured permeability levels simultaneously. In Figure 2.c,2.d, the diagrams

Preprints.org (www.preprints.org) | NOT PEER-REVIEWED | Posted: 23 December 2024 doi:10.20944/preprints202412.1900.v1



show that the theoretical results align with the experimental ones. We found that the real part of permeability increases with low pressure, reching a maximum of 700 (emu) at $P_{Ar}$ = 4.10$^{-3}$ (mbar). It suggests that the variation of permeability with argon pressure ($P_{Ar}$) present a good resonance frequency at low pressure. There is a sign change observed for the real part when the imaginary part reaches its maximum. In this study, we have demonstrated the ability to adjust the resonance frequency in the band 250 MHz - 1 GHz for the deposited thin films. These highly soft ferromagnetic layers (coercive field $H_c < 0.5(0e)$) are particularly interesting for microwave applications due to their adjustable resonance frequency. The reduction in argon pressure observed in the microwave (Figure 2.c,2.d), is caused by augmentation the strength of the anisotropy field coupled with the demagnetization effects. This was accompanied by different magnetic loss spreading. As shown in Figure (2.e,2.f), the measured and simulated values of the imaginary part $\mu''$ of permeability were close across the frequency band 250 MHz - 1 GHz for a concentration of 44%.

The amplitude loss $\mu''$ and the position of the resonance frequency are affected by the damping factor spectra and the width of resonance. Both the initial permeability and the resonance frequency diminish with increasing pressure, Our results are sufficient when compared to Samuel Queste's [17]**.** When the pressure exceeds the value 17.10$^{-3}$ (mbar), the resonance frequency is canceled, and the dissipative parameter $\alpha_{eff}$ is inferior than 0.088. The lower absorption resonance $\mu''$ is important and has a narrow linewidth .These curves show a significant expansion of the of magnetic loss area for low field values [36] **.** The damping coefficient values obtained from theoretical simulations using GLL equation with experimental results are determined. The reduction in pressure is a good way to get a very small coefficient deeply. The resonance frequency appears when the damping coefficient ranges between 0.032 and 0.0885. The LLG model may be used to accurately fit all of these permeability spectra, as shown in Figures. (2.c-2. d-2.e-2.f), which means that the natural resonances occur within these frequency ranges. The measured pressure range spanned from 1.9.10$^{-3}$ (mbar) up to 60.10$^{-3}$ (mbar). As the pressure increases, the permeability spectrum noticeably moves towards a lower frequency, as shown in Figures 3 and 4. Permalloy's trend can be compared to certain more magnetic materials that were earlier investigated by our and other research groups examined[17,24,37].

The influence of pressure and saturation magnetizations of different concentrations seems high, as illustrated in Figure 3.b. We observe a similar behavior in the variation of the saturation magnetization for the three rates. The magnetization decreases as pressure increases. The best Permalloy deposit is below the pressure 17.10$^{-3}$ (mbar) , containing high magnetization. Possibly due to variations in the $Al_2O_3$ concentration gradient, the easy axis was perpendicular to the employed external magnetic field when the $P_{Ar}$ flow rates were equal to or less than 17.10$^{-3}$(mbar). The damping factor, being too low, leads to a slightly damped precession around the new equilibrium position; It is commonly recognized that the primary cause of the decrease in magnetization saturation with pressure. Furthermore, Figure (3.a) displays the $H_k^{Stat}$ and coercivity ($Hc$) values that were attained from the VSM measurement results.

It is widely recognized that $Hc$ is dependent on the magnetization process's reversal modes as well as magnetic anisotropy. But just like in our situation, the coercivity essentially stayed the same while the magnetic anisotropy depicted in Figure (3.a) altered dramatically. While $H_k^{Stat}$ and $H_k^{dyn}$ both rise with pressure, $H_k^{dyn}$ value was greater than $H_k^{Stat}$. This difference, which has also been noted in many other magnetic thin films, can be explained by rotatable magnetic anisotropy [6,38,39] **.** Rotatable magnetic anisotropy is consistently aligned in both direction and magnetization.

Preprints.org (www.preprints.org) | NOT PEER-REVIEWED | Posted: 23 December 2024 doi:10.20944/preprints202412.1900.v1



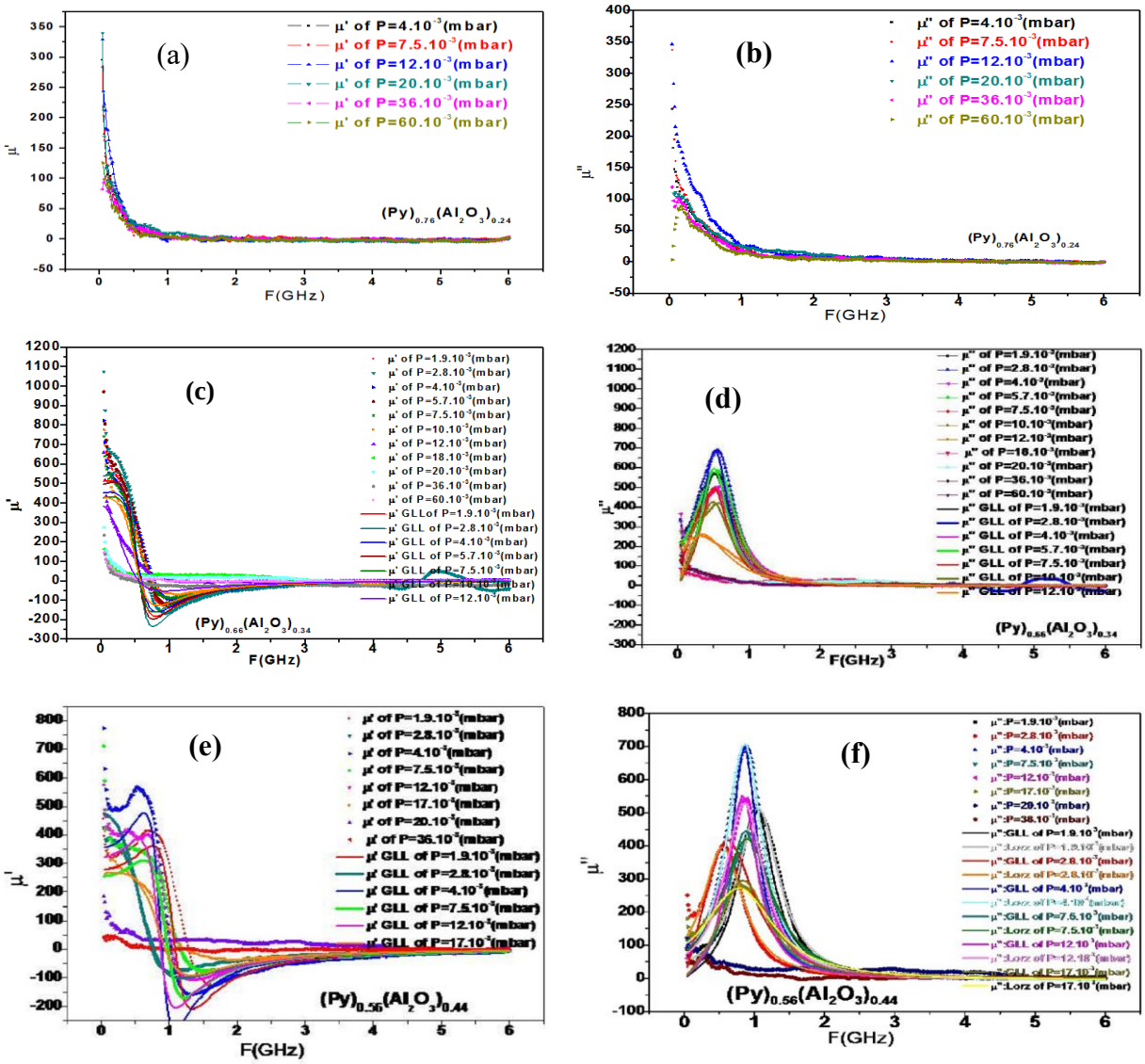


**Figure 2. (a-b-c-d-e-f)** illustrates that theoretical and experimental permeability changes with frequency for various concentrations 24%,34%,44% and pressures at room temperature and constant thickness.

As shown in the $M-H$ loops, when the magnetization is reversed, the anisotropy direction also changes correspondingly[40,41] . The permeability spectra reveal that rotatable magnetic anisotropy exists because there is insufficient tiny stimulated magnetic field to reverse the magnetization, which changes directions at microwave frequencies[42–44]. It is possible to conceptualize this anisotropy as having an energy minimum parallel to a direction of FM magnetization [43], brought about by the existence of ripples or local disorder[45]. The magnetic hysteresis loops of $(Py)_{1-x}(Al_2O_3)_x$ granular film formed at different Argon pressures are displayed in Figure 3.a. The easy axis direction coercivities ($H_{ce}$) of the nanoparticle that was placed at $1.9.10^{-3}$ mbar, $4.10^{-3}$ mbar and $60.10^{-3}$ mbar, got the values 3.58 Oe, 9.31 Oe and 42.93 Oe, successively, show that ($H_{ce}$) increases as Argon pressure rises. Notably, coercivity also augmented in the hard axis direction ($H_{cH}$). The outcomes demonstrate that greater Argon pressure can produce higher ($H_c$). Low Argon pressure films have a specific pressure present, which contributes to their favorable soft magnetic characteristics[46] . The rise in coercivity and anisotropy field fluctuation may be explained by the exchange coupling model[47] , which also successfully describes the soft magnetic characteristics of granular films, nano-crystalline materials, and amorphous films.

Preprints.org (www.preprints.org) | NOT PEER-REVIEWED | Posted: 23 December 2024 doi:10.20944/preprints202412.1900.v1



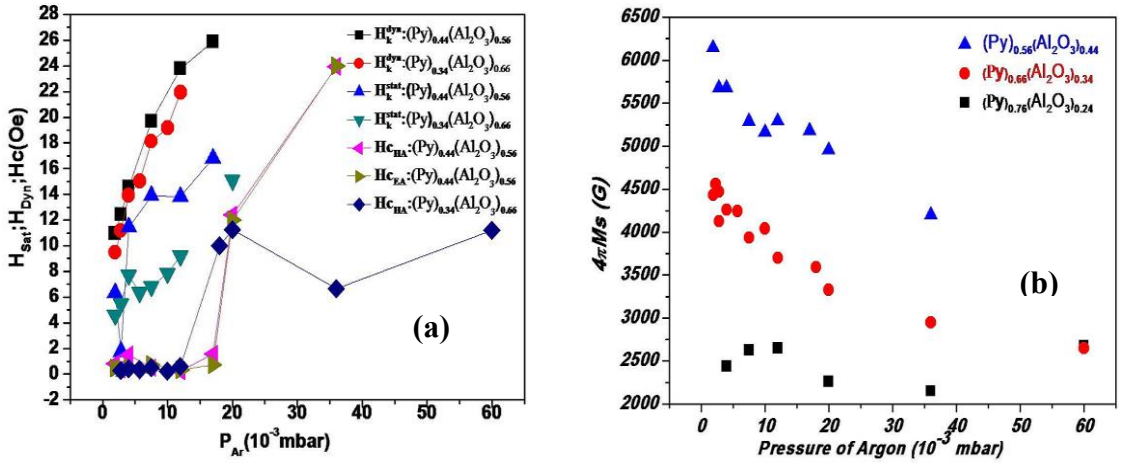


**Figure 3. a.** Dependencies between the static and dynamic anisotropy ($H_k^{stat}$, $H_k^{dyn}$)and coercivities ($H_{ce}$ ; $H_{ch}$) of the various samples deposited at varying sputtering gas pressures.(b) Magnetization dependencies of the various samples deposited at varying pressures of the sputtering gas.

Using the previously indicated parameters, formulae (2)–(3) are used to fit the computed real and imaginary permeability spectra, which are indicated in figures 2.c, 2.d, 2.e, and 2.f. At argon pressures ranging from 1.9.10$^{-3}$ (mbar) to 60.10$^{-3}$ (mbar), the Gilbert dampings that fit are roughly 0.032 and 0.0885 for $(Py)_{1-x}(Al_2O_3)_x$ films. Several sources of damping, such as spin-orbit interactions, magnon interactions, and the spin pumping effect, are identified by the phenomenological quantity known as damping [48–51]. Our magnetic permeability spectra still exhibit a high degree of Gilbert damping, or it can be integrated into Gilbert damping, as demonstrated by the good fit with Eqs (2)–(3) [48].

One would move away from the ideal magnetic characteristics if the pressure in these granular layers were reduced. This offers a plausible explanation for the marginal rise in $H_{ce}$ observed in Figure 4.a,4.b as the pressure of argon is gradually increased. In most cases, lowest $\alpha$ occurs when the optimal static soft magnetic properties are found. Here, the high value of $\alpha$ clearly surpasses the thin film normal range [50] ,demonstrating extrinsic damping effects, such as the inhomogeneity [52] and even the spin-wave contributions [53]. Nevertheless, there is ongoing debate regarding the precise source of these extrinsic damping contributions. The soft magnetic thin films have been the focus of lengthy discussions on various damping mechanisms [18,49,54–57].The phenomenological LLG equation is actually unable to adequately characterize few extrinsic contributions, especially Arias-Mill's TMS [49,50,56,58]. Fig. 4.a illustrates how the effective damping factor $\alpha_{eff}$ and frequency linewidth $\Delta f$ change with argon pressure. It is discovered that and are both insensitive to changes in pressure and that $P_{Ar}$ slightly increases as pressure increases ($\alpha_{eff}$increasing from 0.03 to 0.0885 and from 1.27 to 1.49), nearly meeting the requirement that each component be independently adjusted by changing pressure over a wide frequency range. The following formula can be used to get the frequency linewidth $\Delta f$ [38,42] :

$$\Delta f = \frac{\gamma \alpha_{eff}(2H_k^{dyn} + 4\pi M_s)}{2\pi} \propto \alpha$$

Determining linewidth from experimental data using Lorentzian fits. $\Delta f$ and $\alpha_{eff}$ exhibit comparable increasing tendencies and compare them with the declining tendency of ($\mu_i''$).

Preprints.org (www.preprints.org) | NOT PEER-REVIEWED | Posted: 23 December 2024 doi:10.20944/preprints202412.1900.v1



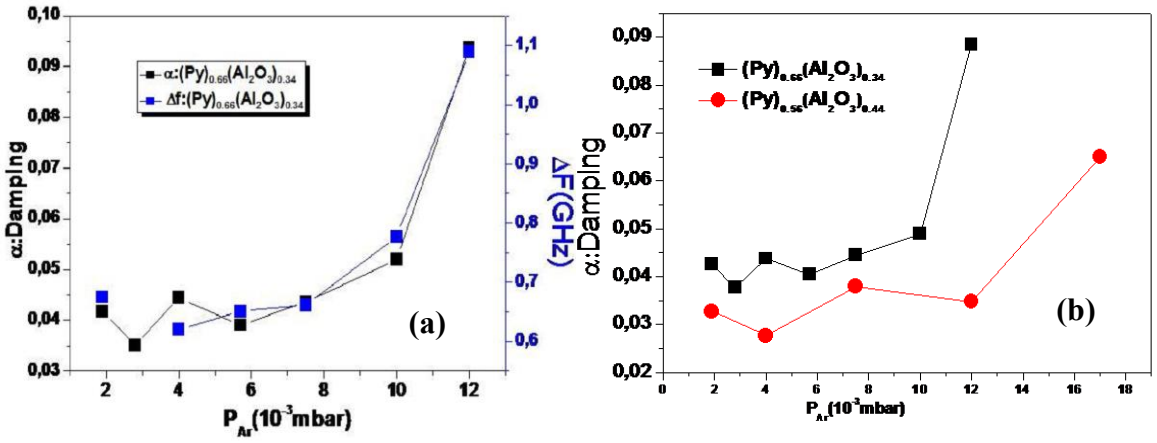


**Figure 4. (a)** Line-width and the damping of the 34% and (b) the damping as a function of Argon pressure respectively for various studied compositions.

From Figure 5-a, we deduced that the frequency never appear at the charge rate 24% , regardless of the pressure. In contrast, in the cases of 34 and 44% , the frequency increases with concentration : which indicates the existence of a resonance frequency. Figure 5.a illustrates how the actual component of permeability rises (from 60 to 800). Correspondingly, the resonance frequency decreases (from 934 to 517MHz) with argon pressure. We note that the resonance frequency at 44% is higher than that at 34% , indicating a good quality of our samples. The ($f_{FMR}$) theory and ($f_{Lor}$) align with the experimental ($f_{FMR}$) in the pressure range between 1.9.10$^{-3}$ (mbar) and 60.10$^{-3}$ (mbar).

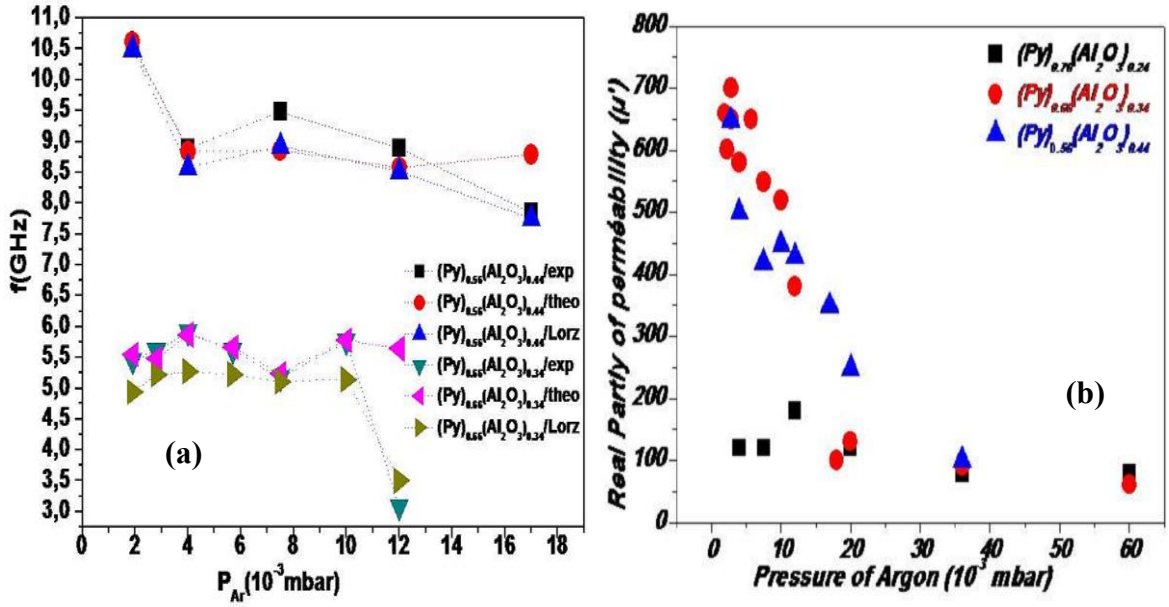


**Figure 5. a):** Frequency dependence on the gas pressure spraying (argon).(b)relationship among the gas pressure spraying (argon) and the real part of the permeability.

Figure 6.a and 6.b illustrate the increase in Line-width Δf and d amping as pressure increases for thin-films manufactured at different argon pressures, demonstrating remarkable tenability.

Accordingly, the imaginary permeability increases under pressure till saturation. The damping value is lowest when the softest magnetic characteristics are found, as indicated by the damping change tendency being almost equal to that of ($H_C$). It is evident that when the gas Argon pressure rises, the damping increases significantly. It seems generally that the situation with the best static soft magnetic characteristics yields the lowest Damping. The investigation indicates inversely scaling of

Preprints.org (www.preprints.org) | NOT PEER-REVIEWED | Posted: 23 December 2024 doi:10.20944/preprints202412.1900.v1



the inherent Gilbert damping $\alpha$ [59–61]with varied pressures, where the supplied argon pressure ranges from $4.10^{-3}$ to $60.10^{-3}$ mbar. As a phenomenological characteristic, damping suggests many types of physical sources, such as interactions between magnons and spin-orbit interactions [49,56] . An explanation of how pressure impacts the static soft magnetic properties in response to thin-film stress has been published [62–65]. By identifying the peak point during the permeability spectrum experiment, able to approximate the FMR frequency; however, this method is not precise when dealing with broad frequency line-width. Therefore, The fitting curves in Figure (2.c,2.f) are implemented for identifying the FMR frequency ($f_{FMR}$) for increased precision.

Figure 6.c illustrates how the FMR frequency and frequency line-width change with pressure. Specifically, the following method can be used to obtain ($f_{FMR}$) using Kittel's equation[66]:

$$f_{FMR} = \frac{\gamma}{2\pi}\sqrt{\left(H_k^{dyn} + 4\pi M_s\right)H_k^{dyn}}$$

According to Kittel's equation [67–75], this increase in magnetic anisotropy induce to rise in the ferromagnetic resonance frequency, which is coherent with the outcome seen in Figure 6.c. According to the illustration, the increasing tendencies of $f_{FMR}$, $f_{Lor}$, and $\Delta f$ are similar to each other, while $\alpha_{eff}$ is increasing tendency is illustrated in Figure 6.a,6.b. $H_k^{dyn}$, Damping, $f_{FMR}$, and frequency line-width are among the fitting parameters that are illustrates in Figures 6.a and 6.b, consecutively. in contrast to the comparable anisotropy dynamic values $H_k^{dyn}$, which were marginally greater and had a similar tendency to the anisotropy static $H_k^{Stat}$ depicted in Figure 5.a. The variations between them were attributed to the influence of magnetic ripple fields [76] and was documented in numerous academic publications[77–80].

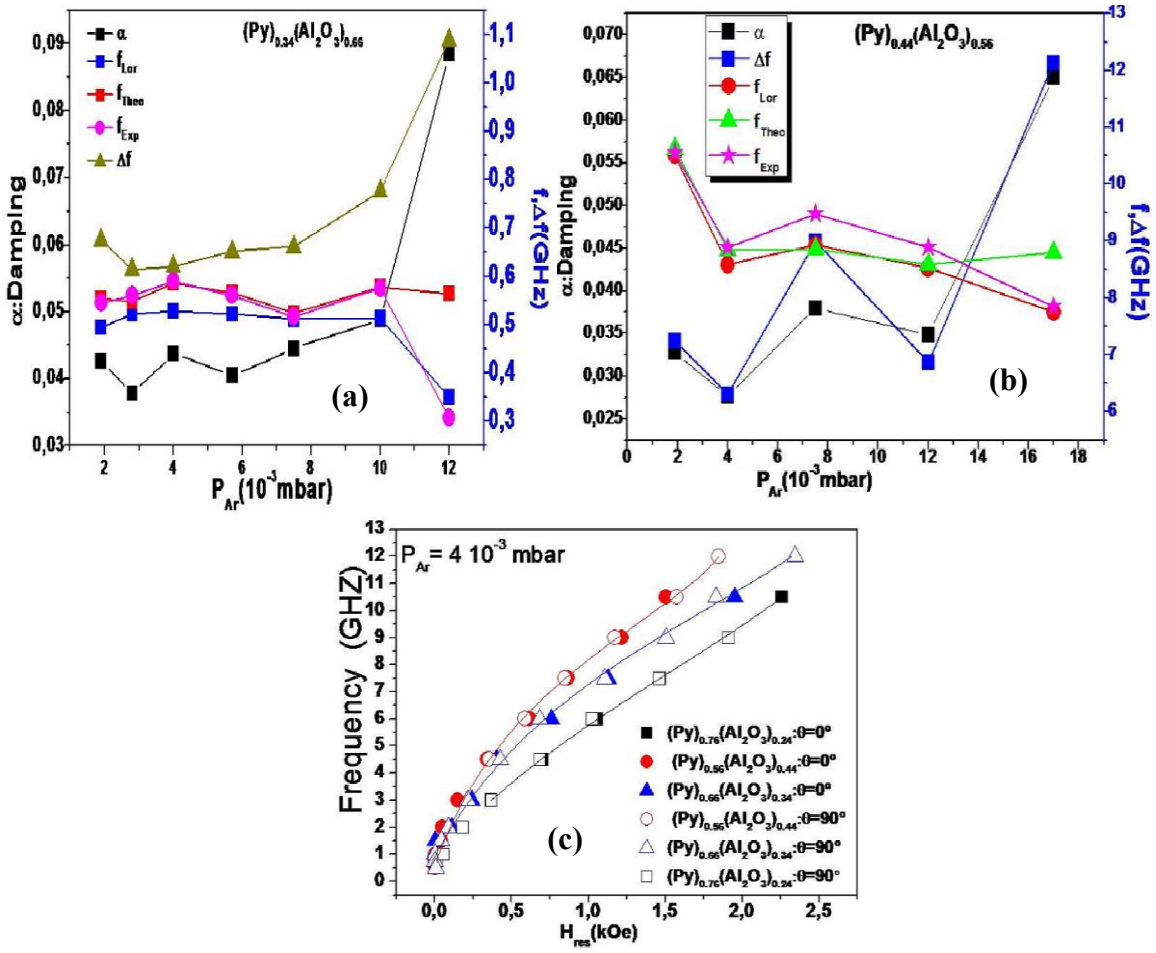


**Figure 6.** : Dependence of Line-width, frequency and the damping as a function of the gas pressure spraying (Argon) at different concentrations 34% (a) and 44% (b), respectively, and (c) Evolution

Preprints.org (www.preprints.org) | NOT PEER-REVIEWED | Posted: 23 December 2024 doi:10.20944/preprints202412.1900.v1



of the resonance frequency depending on the resonance field of Py-$Al_2O_3$ for various Pressures in Plan θ=0° and θ=90°.

## 5. Conclusions

The permeability spectra obtained from the Gilbert model and considering a dynamic field along the axis of hard magnetization, were compared with those obtained experimentally, which were in a good agreement. The resonance frequency and the permeability in the same method varied depending on the argon pressure. An increase in pressure caused the effective field to rise, resulting in a larger permeability. When the dissipative parameter $\alpha_{eff}$ was smaller, the resonance absorption was important, resulting in narrow linewidth . However, measurements in the frequency domain have been shown to offere better guarantees of validity.

**Funding:** The research is not being funded by outside sources.

**Acknowledgments:** The authors thank the Condensed Matter Physics and Nanomaterials for Renewable Energy, Agadir and LPMC, Kenitra Morocco for its relevant help regarding software.

**Conflicts of Interest:** The authors declare no conflict of interest.

**Declaration of Competing Interest:** The authors affirm that none of the work described in this publication may have been influenced by any known competing financial interests or personal relationships.

## References

1. Hayakawa, Y.; Makino, A.; Fujimori, H.; Inoue, A. High Resistive Nanocrystalline Fe-M-O (M=Hf, Zr, Rare-Earth Metals) Soft Magnetic Films for High-Frequency Applications (Invited). *J Appl Phys* 1997, *81*, 3747–3752, doi:10.1063/1.365498.
2. Ohnuma, S.; Masumoto, T. High Frequency Magnetic Properties and GMR Effect of Nano-Granular Magnetic Thin Films. *Scr Mater* 2001, *44*, 1309–1313, doi:10.1016/S1359-6462(01)00699-6.
3. Tsepelev, V.S.; Starodubtsev, Y.N. Nanocrystalline Soft Magnetic Iron-Based Materials from Liquid State to Ready Product. *Nanomaterials* 2021, *11*, 1–39.
4. Zhou, J.; Zhang, X.; Wang, S.; Wang, H.; Li, J. Magnetic Properties, Microwave Characteristics, and Thermal Stability of the FeCoAlN Films. *J Mater Eng Perform* 2010, *19*, 737–742, doi:10.1007/s11665-009-9529-0.
5. Yao, D.; Ge, S.; Zhou, X.; Zuo, H. Grain Size Dependence of Coercivity in Magnetic Metal-Insulator Nanogranular Films with Uniaxial Magnetic Anisotropy. *J Appl Phys* 2010, *107*, 073902, doi:10.1063/1.3357399.
6. Phuoc, N.N.; Hung, L.T.; Ong, C.K. FeCoHfN Thin Films Fabricated by Co-Sputtering with High Resonance Frequency. *J Alloys Compd* 2011, *509*, 4010–4013, doi:10.1016/J.JALLCOM.2010.12.208.
7. Kong, L.H.; Chen, R.R.; Song, T.T.; Gao, Y.L.; Zhai, Q.J. Magnetic Characterization of Dual Phase FeZrB Soft Magnetic Alloy. *J Magn Magn Mater* 2011, *323*, 3285–3289, doi:10.1016/J.JMMM.2011.07.037.
8. Yao, D.; Ge, S.; Zhang, B.; Zuo, H.; Zhou, X. Fabrication and Magnetism of Fe65Co35-MgF2 Granular Films for High Frequency Application. *J Appl Phys* 2008, *103*, doi:10.1063/1.2932076.
9. Landau, L.; Lifshitz, E. On the Theory of the Dispersion of Magnetic Permeability in Ferromagnetic Bodies. *Phys. Z. Sowjetunion* 1935, *8*, 101–114.
10. Su, J.; Niekiel, F.; Fichtner, S.; Kirchhof, C.; Meyners, D.; Quandt, E.; Wagner, B.; Lofink, F. Frequency Tunable Resonant Magnetoelectric Sensors for the Detection of Weak Magnetic Field. *Journal of Micromechanics and Microengineering* 2020, *30*, 075009, doi:10.1088/1361-6439/ab8dd0.
11. Ren, W.; Li, J.; Liu, G.; Chen, J.; Chen, S.; Gu, Z.; Li, J.; Li, J.; Gao, Y. Design and Optimization of a BAW Magnetic Sensor Based on Magnetoelectric Coupling. *Micromachines (Basel)* 2022, *13*, doi:10.3390/mi13020206.
12. Salahun, E.; Tanné, G.; Quéffélec, P.; Lefloc'h, M.; Adenot, A. -L.; Acher, O. Application of Ferromagnetic Composite in Different Planar Tunable Microwave Devices. *Microw Opt Technol Lett* 2001, *30*, 272–276, doi:10.1002/mop.1288.

Preprints.org (www.preprints.org) | NOT PEER-REVIEWED | Posted: 23 December 2024 doi:10.20944/preprints202412.1900.v1




13. Wang, D.; Zhang, J.; Cui, S.; Bie, Z.; Song, K.; Zhu, C.; Matveevich, M.I. Modern Advances in Magnetic Materials of Wireless Power Transfer Systems: A Review and New Perspectives. *Nanomaterials* 2022, *12*, doi:10.3390/nano12203662.
14. Maemura, M.; Kurpat, T.; Kimura, K.; Suzuki, T.; Hashimoto, T. Improvement of the Power Transfer Efficiency of a Dynamic Wireless Power Transfer System via Spatially Distributed Soft Magnetic Materials. In Proceedings of the 2022 Wireless Power Week (WPW); July 2022; pp. 332–337.
15. Acher, O.; Vermeulen, J.L.; Lucas, A.; Baclet, Ph.; Kazandjoglou, J.; Peuzin, J.C. Direct Measurement of Permeability up to 3 GHz of Co-Based Alloys under Tensile Stress. *J Appl Phys* 1993, *73*, 6162–6164, doi:10.1063/1.352736.
16. Grove, W.R. LXXIX. *On the Electro-Chemical Polarity of Gases*. *The London, Edinburgh, and Dublin Philosophical Magazine and Journal of Science* 1852, *4*, 498–514, doi:10.1080/14786445208647172.
17. Ledieu, M.; Schoenstein, F.; Le Gallou, J.-H.; Valls, O.; Queste, S.; Duverger, F.; Acher, O. Microwave Permeability Spectra of Ferromagnetic Thin Films over a Wide Range of Temperatures. *J Appl Phys* 2003, *93*, 7202–7204, doi:10.1063/1.1555902.
18. Gilbert, T.L. Classics in Magnetics A Phenomenological Theory of Damping in Ferromagnetic Materials. *IEEE Trans Magn* 2004, *40*, 3443–3449, doi:10.1109/TMAG.2004.836740.
19. Salahun, E.; Tanné, G.; Quéffélec, P.; Lefloc'h, M.; Adenot, A. -L.; Acher, O. Application of Ferromagnetic Composite in Different Planar Tunable Microwave Devices. *Microw Opt Technol Lett* 2001, *30*, 272–276, doi:10.1002/mop.1288.
20. Kuanr, B.K.; Camley, R.E.; Celinski, Z. Exchange Bias of NiO/NiFe: Linewidth Broadening and Anomalous Spin-Wave Damping. *J Appl Phys* 2003, *93*, 7723–7725, doi:10.1063/1.1557964.
21. Spenato, D.; Pogossian, S.P.; Dekadjevi, D.T.; Youssef, J. Ben Study of Dynamic Properties and Magnetic Anisotropies of NiFe/MnPt in the Critical Thickness Range. *J Phys D Appl Phys* 2007, *40*, 3306–3313, doi:10.1088/0022-3727/40/11/008.
22. Ge, S.; Yao, D.; Yamaguchi, M.; Yang, X.; Zuo, H.; Ishii, T.; Zhou, D.; Li, F. Microstructure and Magnetism of FeCo–SiO 2 Nano-Granular Films for High Frequency Application. *J Phys D Appl Phys* 2007, *40*, 3660–3664, doi:10.1088/0022-3727/40/12/016.
23. Liu, Y.; Chen, L.; Tan, C.Y.; Liu, H.J.; Ong, C.K. Broadband Complex Permeability Characterization of Magnetic Thin Films Using Shorted Microstrip Transmission-Line Perturbation. *Review of Scientific Instruments* 2005, *76*, doi:10.1063/1.1935429.
24. Phuoc, N.N.; Chai, G.; Ong, C.K. Temperature-Dependent Dynamic Magnetization of FeCoHf Thin Films Fabricated by Oblique Deposition. *J Appl Phys* 2012, *112*, doi:10.1063/1.4763361.
25. Phuoc, N.N.; Ong, C.K. Anomalous Temperature Dependence of Magnetic Anisotropy in Gradient-Composition Sputterred Thin Films. *Advanced Materials* 2013, *25*, 980–984, doi:10.1002/adma.201203995.
26. Phuoc, N.N.; Ong, C.K. Observation of Magnetic Anisotropy Increment with Temperature in Composition-Graded FeCoZr Thin Films. *Appl Phys Lett* 2013, *102*, doi:10.1063/1.4808165.
27. Phuoc, N.N.; Chapon, P.; Acher, O.; Ong, C.K. Large Magneto-Elastic Anisotropy Enhancement with Temperature in Composition-Graded FeCoTa Thin Films. *J Appl Phys* 2013, *114*, doi:10.1063/1.4825225.
28. Phuoc, N.N.; Ong, C.K. Gradient-Composition Sputtering: An Approach to Fabricate Magnetic Thin Films With Magnetic Anisotropy Increased With Temperature. *IEEE Trans Magn* 2014, *50*, 1–6, doi:10.1109/TMAG.2013.2296936.
29. Kipgen, L.; Fulara, H.; Raju, M.; Chaudhary, S. In-Plane Magnetic Anisotropy and Coercive Field Dependence upon Thickness of CoFeB. *J Magn Magn Mater* 2012, *324*, 3118–3121, doi:10.1016/j.jmmm.2012.05.012.
30. Zhang, H.; Li, Y.-Y.; Yang, M.-Y.; Zhang, B.; Yang, G.; Wang, S.-G.; Wang, K.-Y. Tuning the Magnetic Anisotropy of CoFeB Grown on Flexible Substrates. *Chinese Physics B* 2015, *24*, 077501, doi:10.1088/1674-1056/24/7/077501.
31. Camarero, J.; Sort, J.; Hoffmann, A.; García-Martín, J.M.; Dieny, B.; Miranda, R.; Nogués, J. Origin of the Asymmetric Magnetization Reversal Behavior in Exchange-Biased Systems: Competing Anisotropies. *Phys Rev Lett* 2005, *95*, 057204, doi:10.1103/PhysRevLett.95.057204.

Preprints.org (www.preprints.org) | NOT PEER-REVIEWED | Posted: 23 December 2024 doi:10.20944/preprints202412.1900.v1




32. Liu, M.; Du, S.; Wang, F.; Adam, R.; Li, Q.; Ma, X.; Guo, X.; Chen, X.; Yu, J.; Song, Y.; et al. Influence of Surface Pinning in the Domain on the Magnetization Dynamics in Permalloy Striped Domain Films. *J Alloys Compd* 2021, *869*, 159327, doi:10.1016/j.jallcom.2021.159327.
33. Lamy, Y.; Viala, B. NiMn, IrMn, and NiO Exchange Coupled CoFe Multilayers for Microwave Applications. *IEEE Trans Magn* 2006, *42*, 3332–3334, doi:10.1109/TMAG.2006.878871.
34. Jiang, C.; Xue, D.; Sui, W. Broadband Microwave Absorption in [NiFe/FeMn]n Exchange-Coupled Multilayer Films. *Thin Solid Films* 2011, *519*, 2527–2530, doi:10.1016/j.tsf.2010.11.030.
35. Phuoc, N.N.; Xu, F.; Ma, Y.; Ong, C.K. Permalloy–FeMn Exchange-Biased Multilayers Grown on Flexible Substrates for Microwave Applications. *J Magn Magn Mater* 2009, *321*, 2685–2690, doi:10.1016/j.jmmm.2009.03.073.
36. Mallegol, S. Caractérisation et Application de Matériaux Composites Nanostructures à La Réalisation de Dispositifs Hyperfréquences Non Réciproques , Université de Bretagne occidentale-Brest, 2003.
37. Hung, L.T.; Phuoc, N.N.; Wang, X.-C.; Ong, C.K. Temperature Dependence Dynamical Permeability Characterization of Magnetic Thin Film Using Near-Field Microwave Microscopy. *Review of Scientific Instruments* 2011, *82*, doi:10.1063/1.3622850.
38. Phuoc, N.N.; Xu, F.; Ong, C.K. Tuning Magnetization Dynamic Properties of Fe–SiO2 Multilayers by Oblique Deposition. *J Appl Phys* 2009, *105*, doi:10.1063/1.3143042.
39. Rantschler, J.O.; Alexander, C. Ripple Field Effect on High-Frequency Measurements of FeTiN Films. *J Appl Phys* 2003, *93*, 6665–6667, doi:10.1063/1.1556097.
40. Olamit, J.; Liu, K. Rotational Hysteresis of the Exchange Anisotropy Direction in Co/FeMn Thin Films. *J Appl Phys* 2007, *101*, doi:10.1063/1.2694378.
41. Yang, P.Y.; Song, C.; Fan, B.; Zeng, F.; Pan, F. The Role of Rotatable Anisotropy in the Asymmetric Magnetization Reversal of Exchange Biased NiO/Ni Bilayers. *J Appl Phys* 2009, *106*, doi:10.1063/1.3157176.
42. Phuoc, N.N.; Ong, C.K. Influence of Ferromagnetic Thickness on Dynamic Anisotropy in Exchange-Biased MnIr/FeCo Multilayered Thin Films. *Physica B Condens Matter* 2011, *406*, 3514–3518, doi:10.1016/J.PHYSB.2011.05.063.
43. McCord, J.; Mattheis, R.; Elefant, D. Dynamic Magnetic Anisotropy at the Onset of Exchange Bias: The $\mathrm{Ni}\mathrm{Fe}/\mathrm{Ir}\mathrm{Mn}$ Ferromagnet/Antiferromagnet System. *Phys Rev B* 2004, *70*, 94420, doi:10.1103/PhysRevB.70.094420.
44. McMichael, R.D.; Lee, C.G.; Bonevich, J.E.; Chen, P.J.; Miller, W.; Egelhoff Jr., W.F. Strong Anisotropy in Thin Magnetic Films Deposited on Obliquely Sputtered Ta Underlayers. *J Appl Phys* 2000, *88*, 3561–3564, doi:10.1063/1.1289517.
45. Gilmore, K.; Stiles, M.D.; Seib, J.; Steiauf, D.; Fähnle, M. Anisotropic Damping of the Magnetization Dynamics in Ni, Co, and Fe. *Phys Rev B* 2010, *81*, 174414, doi:10.1103/PhysRevB.81.174414.
46. Bai, D.Z.; Zhu, J.-G.; Yu, W.; Bain, J.A. Micromagnetic Simulation of Effect of Stress-Induced Anisotropy in Soft Magnetic Thin Films. *J Appl Phys* 2004, *95*, 6864–6866, doi:10.1063/1.1667445.
47. Rudeichuk, T.; Olekšáková, D.; Maciaszek, R.; Matysiak, W.; Kollár, P. Exploring the Impact of Different Milling Parameters of Fe/SiO2 Composites on Their Structural and Magnetic Properties. *Materials* 2024, *17*, doi:10.3390/ma17040862.
48. Youssef, J. Ben; Vukadinovic, N.; Billet, D.; Labrune, M. Thickness-Dependent Magnetic Excitations in Permalloy Films with Nonuniform Magnetization. *Phys Rev B* 2004, *69*, 174402.
49. Zakeri, Kh.; Lindner, J.; Barsukov, I.; Meckenstock, R.; Farle, M.; von Hörsten, U.; Wende, H.; Keune, W.; Rocker, J.; Kalarickal, S.S.; et al. Spin Dynamics in Ferromagnets: Gilbert Damping and Two-Magnon Scattering. *Phys Rev B* 2007, *76*, 104416, doi:10.1103/PhysRevB.76.104416.
50. Tserkovnyak, Y.; Brataas, A.; Bauer, G.E.W. Enhanced Gilbert Damping in Thin Ferromagnetic Films. *Phys Rev Lett* 2002, *88*, 117601, doi:10.1103/PhysRevLett.88.117601.
51. Gerrits, Th.; Schneider, M.L.; Silva, T.J. Enhanced Ferromagnetic Damping in Permalloy/Cu Bilayers. *J Appl Phys* 2006, *99*, doi:10.1063/1.2159076.
52. Bonin, R.; Schneider, M.L.; Silva, T.J.; Nibarger, J.P. Dependence of Magnetization Dynamics on Magnetostriction in NiFe Alloys. *J Appl Phys* 2005, *98*, 123904.

Preprints.org (www.preprints.org) | NOT PEER-REVIEWED | Posted: 23 December 2024 doi:10.20944/preprints202412.1900.v1




53. Counil, G.; Kim, J.-V.; Devolder, T.; Chappert, C.; Shigeto, K.; Otani, Y. Spin Wave Contributions to the High-Frequency Magnetic Response of Thin Films Obtained with Inductive Methods. *J Appl Phys* 2004, *95*, 5646–5652, doi:10.1063/1.1697641.
54. Lenz, K.; Wende, H.; Kuch, W.; Baberschke, K.; Nagy, K.; Jánossy, A. Two-Magnon Scattering and Viscous Gilbert Damping in Ultrathin Ferromagnets. *Phys Rev B* 2006, *73*, 144424, doi:10.1103/PhysRevB.73.144424.
55. Kuanr, B.K.; Camley, R.E.; Celinski, Z. Extrinsic Contribution to Gilbert Damping in Sputtered NiFe Films by Ferromagnetic Resonance. *J Magn Magn Mater* 2005, *286*, 276–281, doi:10.1016/j.jmmm.2004.09.080.
56. Mills, D.L.; Arias, R. The Damping of Spin Motions in Ultrathin Films: Is the Landau–Lifschitz–Gilbert Phenomenology Applicable? *Physica B Condens Matter* 2006, *384*, 147–151, doi:10.1016/j.physb.2006.05.209.
57. Kalarickal, S.S.; Krivosik, P.; Das, J.; Kim, K.S.; Patton, C.E. Microwave Damping in Polycrystalline Fe-Ti-N Films: Physical Mechanisms and Correlations with Composition and Structure. *Phys Rev B* 2008, *77*, 054427, doi:10.1103/PhysRevB.77.054427.
58. Lenz, K.; Wende, H.; Kuch, W.; Baberschke, K.; Nagy, K.; Jánossy, A. Two-Magnon Scattering and Viscous Gilbert Damping in Ultrathin Ferromagnets. *Phys Rev B* 2006, *73*, 144424, doi:10.1103/PhysRevB.73.144424.
59. Kalarickal, S.S.; Krivosik, P.; Das, J.; Kim, K.S.; Patton, C.E. Microwave Damping in Polycrystalline Fe-Ti-N Films: Physical Mechanisms and Correlations with Composition and Structure. *Phys Rev B* 2008, *77*, 054427, doi:10.1103/PhysRevB.77.054427.
60. Huaping Zuo; Shihui Ge; Zhenkun Wang; Yuhua Xiao; Dongsheng Yao Soft Magnetic Properties and High-Frequency Characteristics in FeCoSi/Native-Oxide Multilayer Films. *IEEE Trans Magn* 2008, *44*, 3111–3114, doi:10.1109/TMAG.2008.2001626.
61. Xu, X.; Jin, L.; Wen, T.; Liao, Y.; Tang, X.; Zhang, H.; Zhong, Z. Effects of Substrate Annealing on Uniaxial Magnetic Anisotropy and Ferromagnetic Resonance Frequency of Ni80Fe20 Films Deposited on Self-Organized Periodically Rippled Sapphire Substrates. *Vacuum* 2021, *186*, 110047, doi:10.1016/j.vacuum.2021.110047.
62. Srinivas, K.; Manivel Raja, M.; Sridhara Rao, D. V.; Kamat, S. V. Effect of Sputtering Pressure and Power on Composition, Surface Roughness, Microstructure and Magnetic Properties of as-Deposited Co2FeSi Thin Films. *Thin Solid Films* 2014, *558*, 349–355, doi:10.1016/J.TSF.2014.02.052.
63. Peng, B.; Zhang, W.L.; Xie, Q.Y.; Zhang, W.X.; Jiang, H.C. Effect of Sputtering Pressure on Microstructure and Magnetic Properties of Amorphous FeCoSiB Films. *J Non Cryst Solids* 2013, *365*, 59–62, doi:10.1016/j.jnoncrysol.2013.01.028.
64. Zhou, C.; Li, T.; Wei, X.; Yan, B. Effect of the Sputtering Power on the Structure, Morphology and Magnetic Properties of Fe Films. *Metals (Basel)* 2020, *10*, 1–11, doi:10.3390/MET10070896.
65. Ellis, E.A.I.; Chmielus, M.; Han, S.; Baker, S.P. Effect of Sputter Pressure on Microstructure and Properties of β-Ta Thin Films. *Acta Mater* 2020, *183*, 504–513, doi:10.1016/j.actamat.2019.10.056.
66. Kittel, C. On the Theory of Ferromagnetic Resonance Absorption. *Physical Review* 1948, *73*, 155–161, doi:10.1103/PhysRev.73.155.
67. McMichael, R.D.; Twisselmann, D.J.; Kunz, A. Localized Ferromagnetic Resonance in Inhomogeneous Thin Films. *Phys Rev Lett* 2003, *90*, 227601, doi:10.1103/PhysRevLett.90.227601.
68. Pei Zou; Yu, W.; Bain, J.A. Influence of Stress and Texture on Soft Magnetic Properties of Thin Films. *IEEE Trans Magn* 2002, *38*, 3501–3520, doi:10.1109/TMAG.2002.802705.
69. Kittel, C. Interpretation of Anomalous Larmor Frequencies in Ferromagnetic Resonance Experiment. *Physical Review* 1947, *71*, 270–271, doi:10.1103/PhysRev.71.270.2.
70. Chen, Y.; Wang, J.; Liu, M.; Lou, J.; Sun, N.X.; Vittoria, C.; Harris, V.G. Giant Magnetoelectric Coupling and E-Field Tunability in a Laminated Ni2MnGa/Lead-Magnesium-Niobate-Lead Titanate Multiferroic Heterostructure. *Appl Phys Lett* 2008, *93*, doi:10.1063/1.2986480.
71. Lou, J.; Reed, D.; Pettiford, C.; Liu, M.; Han, P.; Dong, S.; Sun, N.X. Giant Microwave Tunability in FeGaB/Lead Magnesium Niobate-Lead Titanate Multiferroic Composites. *Appl Phys Lett* 2008, *92*, doi:10.1063/1.2952828.
72. Li, S.; Xue, Q.; Duh, J.-G.; Du, H.; Xu, J.; Wan, Y.; Li, Q.; Lü, Y. Driving Ferromagnetic Resonance Frequency of FeCoB/PZN-PT Multiferroic Heterostructures to Ku-Band via Two-Step Climbing: Composition Gradient Sputtering and Magnetoelectric Coupling. *Sci Rep* 2014, *4*, 7393, doi:10.1038/srep07393.

Preprints.org (www.preprints.org) | NOT PEER-REVIEWED | Posted: 23 December 2024 doi:10.20944/preprints202412.1900.v1




73. Li, S.; Xue, Q.; Du, H.; Xu, J.; Li, Q.; Shi, Z.; Gao, X.; Liu, M.; Nan, T.; Hu, Z.; et al. Large E-Field Tunability of Magnetic Anisotropy and Ferromagnetic Resonance Frequency of Co-Sputtered Fe50Co50-B Film. *J Appl Phys* 2015, *117*, doi:10.1063/1.4906752.
74. Phuoc, N.N.; Ong, C.K. Electric Field Modulation of Ultra-High Resonance Frequency in Obliquely Deposited [Pb(Mg1/3Nb2/3)O3]0.68-[PbTiO3]0.32(011)/FeCoZr Heterostructure for Reconfigurable Magnetoelectric Microwave Devices. *Appl Phys Lett* 2014, *105*, doi:10.1063/1.4890411.
75. Phuoc, N.N.; Ong, C.K. Electric Field Control of Microwave Characteristics in Composition-Graded FeCoTa Film Grown onto [Pb(Mg1/3Nb2/3)O3]0.68-[PbTiO3]0.32(011) Crystal. *Appl Phys Lett* 2014, *105*, doi:10.1063/1.4891048.
76. Hoffmann, H. Magnetic Properties of Thin Ferromagnetic Films in Relation to Their Structure. *Thin Solid Films* 1979, *58*, 223–233, doi:10.1016/0040-6090(79)90241-4.
77. Platt, C.L.; Berkowitz, A.E.; Smith, D.J.; McCartney, M.R. Correlation of Coercivity and Microstructure of Thin CoFe Films. *J Appl Phys* 2000, *88*, 2058–2062, doi:10.1063/1.1305833.
78. Liu, X.-L.; Wang, L.-S.; Luo, Q.; Xu, L.; Yuan, B.-B.; Peng, D.-L. Preparation and High-Frequency Soft Magnetic Property of FeCo-Based Thin Films. *Rare Metals* 2016, *35*, 742–746, doi:10.1007/s12598-015-0574-6.
79. Pan, L.; Xie, H.; Cheng, X.; Zhao, C.; Feng, H.; Cao, D.; Wang, J.; Liu, Q. Tuning the Ferromagnetic Resonance Frequency of Soft Magnetic Film by Patterned Permalloy Micro-Stripes with Stripe-Domain. *J Magn Magn Mater* 2018, *457*, 46–51, doi:10.1016/j.jmmm.2018.02.060.
80. Sun, J.; Ren, J.; Li, J.; Huang, Y. Measurement and Analysis of Magnetic Properties of Permalloy for Magnetic Shielding Devices under Different Temperature Environments. *Materials* 2023, *16*, 3253, doi:10.3390/ma16083253.


**Disclaimer/Publisher's Note:** The statements, opinions and data contained in all publications are solely those of the individual author(s) and contributor(s) and not of MDPI and/or the editor(s). MDPI and/or the editor(s) disclaim responsibility for any injury to people or property resulting from any ideas, methods, instructions or products referred to in the content.